J. Fluid Mech. (1987), *vol.* 185, *pp.* 235–248
Printed in Great Britain

Instability and breaking of a solitary wave

By M. TANAKA†, J. W. DOLD, M. LEWY AND D. H. PEREGRINE
School of Mathematics, University of Bristol, University Walk, Bristol BS8 1TW, UK

(Received 16 November 1986 and in revised form 13 April 1987)

The result of a linear stability calculation of solitary waves which propagate steadily along the free surface of a liquid layer of constant depth is examined numerically by employing a time-stepping scheme based on a boundary-integral method. The initial growth rate that is found for sufficiently small perturbations agrees well with the growth rate expected from the linear stability calculation. In calculating the later 'nonlinear' stage of the instability, it is found that two distinct types of long-time evolution are possible. These depend only on the sign of the unstable normal-mode perturbation that is superimposed initially on the steady wave. The growth of the perturbation ultimately leads to breaking for one sign. Unexpectedly, for the opposite sign, there is a monotonic decrease in the total height of the wave. In this latter case there is a smooth evolution to a stable solitary wave of lesser amplitude but very nearly the same energy.

1. Introduction

The linear stability problem for a solitary wave with an arbitrary amplitude which propagates along the free surface of a liquid layer of constant depth was investigated by Tanaka (1986). His results show that for a solitary wave with an amplitude less than a_e the only normal-mode perturbation is the trivial one corresponding to a pure phase shift. Note that the phase speed and most of the integral properties of the steady solitary wave such as the total energy and mass do not vary monotonically with amplitude. The amplitude/depth ratio at which the total energy is a maximum is here denoted by a_e. On the other hand, for solitary waves of amplitude larger than a_e, Tanaka showed that there are at least two non-trivial normal modes, one growing and one decaying. He was also able to calculate the growth-rate eigenvalues and the eigenfunctions of these modes.

Tanaka found the critical amplitude at which the steady solitary wave loses its stability difficult to locate accurately with his numerical methods for solving the linearized stability problem. However, he argued that the critical amplitude is precisely the amplitude of energy maximum, a_e and his results certainly did not indicate otherwise. This is also consistent with previous knowledge about 'superharmonic' instabilities of periodic waves on deep water (Tanaka 1983; Longuet-Higgins 1984; Tanaka 1985; Saffman 1985). More recently this coincidence of critical amplitude and amplitude of energy maximum was confirmed analytically by Zufiria & Saffman (1986), not only for the case of solitary waves but also for periodic waves on any finite depth by using Zakharov's Hamiltonian formulation of water waves.

† On leave from Department of Applied Mathematics, Faculty of Engineering, Gifu University, Gifu 501-11, Japan.

However, all of this work is based on a linear theory of hydrodynamic instability with the assumption that the perturbation is infinitesimally small compared with the basic steady wave. It does not give any information about 'nonlinear' (larger amplitude) growth of the instability; for example, one might ask if the instability leads eventually to breaking. In order to address this problem, the very efficient time-stepping method, recently developed by Dold & Peregrine (1986), has been used to calculate the long-time evolution of the instability. We have concentrated particularly on a solitary wave with the amplitude-to-depth ratio $a = 0.803\,74$ which is well above the energy-maximum level a_e ($= 0.780\,66$).

Section 2 briefly describes the boundary-integral method used for the time integration and the method of calculating the initial solitary wave. A detailed account of the boundary-integral method is in preparation. The linear stage of the instability is investigated in §3 where the initial growth rates of sufficiently small perturbations are compared with the expected growth rate from the linear stability calculation. Section 4 describes the nonlinear stage of the instability for the growing mode. Although a change of sign of the initial normal-mode perturbation to the basic steady solution makes no difference to the linear stability analysis, this change of sign is shown to lead to completely different results. In one case the growth of the perturbation makes the wave profile progressively steepen, until it leads to breaking on a small scale around the crest. In the other case, with the sign of the initial perturbation reversed, the wave profile becomes progressively less steep as the perturbation grows. The height of the wave steadily decreases, and no breaking occurs. Instead the wave evolves into a lower-amplitude solitary wave, and two long small-amplitude waves, one of which propagates in the same direction as the solitary wave, but more slowly, while the other propagates off in the opposite direction. The approach to this final solitary-wave is found to be exponential which, superficially, appears to contradict the finding from linear stability analysis that this wave is stable; here a consistent description is given. A summary of the results and a brief discussion appears in §5.

2. Method of calculation

2.1. *Time-dependent motion*

For two-dimensional, irrotational motion of an incompressible fluid, the velocity field $\boldsymbol{u}(x, y, t)$ can be expressed as the gradient of a velocity potential $\phi(x, y, t)$ which satisfies Laplace's equation,

$$\phi_{xx} + \phi_{yy} = 0, \tag{2.1}$$

throughout the fluid. As a result, given values of ϕ on a surface surrounding the fluid, all values of ϕ within the fluid are uniquely determined. The problem of solving for the motion of a body of fluid can therefore be reduced to that of tracing the evolution of the shape of its boundary together with the velocity potential along the boundary.

The fluid boundary will be considered to consist of a flat impermeable bottom at $y = -h$ and a free surface which may be expressed parametrically as $\boldsymbol{r} = \boldsymbol{R}(\xi)$. (The nature of ξ will be made more specific later.) In complex coordinates, with $z = x + \mathrm{i}y$, we write the boundary as $z = R(\xi)$, where the complex function R has real and imaginary parts $R(\xi) = X(\xi) + \mathrm{i}Y(\xi)$. The corresponding values of the velocity potential at the surface are given by $\phi(X, Y) = \Phi(\xi)$.

The time evolution of $\boldsymbol{R}$ and ϕ is then determined by the kinetic boundary condition

$$\frac{\mathrm{D}\boldsymbol{R}}{\mathrm{D}t} = \boldsymbol{u} = \boldsymbol{\nabla}\phi, \tag{2.2}$$

and the dynamic boundary condition (Bernoulli's equation)

$$\frac{\mathrm{D}\phi}{\mathrm{D}t} = \tfrac{1}{2}\boldsymbol{u}^2 - (p/\rho + gy). \tag{2.3}$$

At the surface, the pressure p takes its constant atmospheric value, and it makes no difference to the motion if this value is defined as zero. Thus, provided that $\boldsymbol{\nabla}\phi$ can be evaluated, these equations supply all of the basic information required for progressively time stepping the fluid motion.

The component of $\boldsymbol{\nabla}\phi$ tangential to the free surface can be calculated without difficulty since values of ϕ are known along the free surface. The normal gradient is less straightforward to evaluate, but it is at this point that the properties of Laplace's equation (2.1) can be exploited. We briefly show how the normal gradient of ϕ can be calculated at the free surface. More detail is given in Dold & Peregrine (1986), who also indicate how (2.2) and (2.3) are extended to yield higher-order methods of time stepping.

Because of Laplace's equation (2.1), it can be seen that the complex gradient of ϕ, defined as $q = \phi_x - \mathrm{i}\phi_y$, is an analytic function of z. An alternative definition of the complex gradient of ϕ at the surface is that

$$q^* = \frac{(\phi_\xi + \mathrm{i}\phi_\nu)\, R_\xi}{|R_\xi|^2} \tag{2.4}$$

where subscript ξ denotes differentiation with respect to ξ, and ϕ_ν is the normal gradient of ϕ scaled by $|R_\xi|$, and * denotes the complex conjugate. Since ϕ_ξ can be found simply by differentiating $\Phi(\xi)$, the problem reduces to that of solving for ϕ_ν.

Also, in terms of q, the zero-vertical-velocity (impermeability) condition at the flat bottom can be expressed as $\mathrm{Im}(q) = 0$. Alternatively, by notionally allowing the fluid to extend below $y = -h$, a reflection condition,

$$q(R^* - 2\mathrm{i}h) = q^*(R) \tag{2.5}$$

can be imposed. Because q is an analytic function of z between the surface $z = R(\xi)$ and its reflection $z = R^*(\xi) - 2\mathrm{i}h$, the principal-value form of Cauchy's integral equation can be applied,

$$q[R(\xi')] = \frac{1}{\pi\mathrm{i}} \int_C \frac{q\,\mathrm{d}z}{z - R(\xi')}, \tag{2.6}$$

where the contour C consists of both the free surface and its reflection, and integration is performed over one anticlockwise circuit. Substituting the definition (2.4) for q gives, after some rearranging,

$$\pi\phi'_\nu = \int \mathrm{Re}\left[\frac{R'_\xi}{R^* - 2\mathrm{i}h - R'} - \frac{R'_\xi}{R - R'}\right]\phi_\xi \,\mathrm{d}\xi - \int \mathrm{Im}\left[\frac{R'_\xi}{R^* - 2\mathrm{i}h - R'} + \frac{R'_\xi}{R - R'}\right]\phi_\nu \,\mathrm{d}\xi, \tag{2.7}$$

where ξ is taken to vary from $-\infty$ to $+\infty$ as x varies from $-\infty$ to $+\infty$, and the prime denotes evaluation at $z = R(\xi')$.

Finally, by identifying ξ as a point-label parameter which, numerically, takes integral values, the following quadrature formula for (2.7) can be deduced:

$$\pi\phi_\nu(\xi') = \sum_\xi A(\xi',\xi)\,\phi_\xi(\xi) - \phi_{\xi\xi}(\xi') + \sum_\xi B(\xi',\xi)\,\phi_\nu(\xi), \tag{2.8}$$

where

$$A+\mathrm{i}B = \left[\frac{R'_\xi}{R^*-2\mathrm{i}h-R'}\right]^* + \begin{cases} \dfrac{R'_\xi}{R'-R} & (\xi \neq \xi'), \\ \dfrac{R_{\xi\xi}}{2R_\xi} & (\xi = \xi)'. \end{cases} \tag{2.9}$$

For a solitary wave propagating in still water, the values of y and q rapidly approach zero as $|x|$ increases. It is sufficient therefore to take the range of ξ such that ϕ_ξ becomes negligibly small at each end of the range. By solving iteratively for ϕ_ν, the gradient $\nabla\phi$ can be calculated, and the motion of the wave continued forward in time using (2.2) and (2.3). This method was used in the case of some of the calculations presented below.

A variation on this approach, which was used in other cases, and found to produce equivalent results when the methods were compared, arises through imposing periodic boundary conditions as described in Dold & Peregrine (1986). Provided that the spatial period was chosen to be large enough for the 'solitary' wave to be bounded by appreciable regions of almost-uniform flow, the imposition of periodicity was found to produce no ill effects.

Time stepping is effected by evaluating a short Taylor series in time for each of Φ, X and Y, together with one backward time difference. This permits fairly large time-step sizes for a required accuracy and reduces the CPU time by a great amount.

A full account of this numerical method is in preparation.

2.2. *Initial data*

The steady solitary-wave solution and normal-mode perturbations are calculated by the method explained in detail in Tanaka (1986). In using these results to provide initial conditions for the fully time-dependent problem, redistribution of the mesh points is necessary.

In Tanaka's method, mesh points are distributed along the free surface of the steady wave such that points are evenly spaced with respect to a variable γ which is related to the velocity potential Φ (measured in the frame of reference moving with the wave) by the relation

$$\frac{\Phi}{ch} = \alpha\gamma + \gamma^m. \tag{2.10}$$

Here, α is a small positive number and m some positive odd integer. (In the present calculation we chose $\alpha = 0.05$ and $m = 5$.) The fluid depth is given by h, and c is the velocity of propagation or phase speed of the wave relative to the fluid far from the wave. This distribution ensures a high density of mesh points around the steep crest where the good resolution is needed and low density in the region far from the crest where the wave varies very smoothly.

Although this distribution was shown to be very efficient in calculating steady solutions and normal modes, it becomes unsuitable as the wave propagates. In the time-dependent problem the Lagrangian computational fluid particles generally

move in the direction of wave propagation much more slowly than the wave itself. This implies that the region of high point density is left behind as the wave proceeds into a region where the points are more sparsely distributed initially. This causes a serious loss of resolution, especially around the steep crest.

In order to maintain a high resolution around the crest at all times, the original mesh points were redistributed using an 11-point polynomial interpolation formula. The new distribution was made such that the arclength Δs between any two adjacent points is proportional to the fluid speed $|q|(=\mathrm{d}\Phi/\mathrm{d}s)$, measured in the frame of reference moving with the wave. For the unperturbed steady wave, this distribution is 'invariant' in the sense that the initial distribution of mesh points is reproduced periodically on the time interval $\Delta s/|q|(=\text{const.})$ (New 1983).

3. Initial growth of perturbations

The initial condition used for following the unstable evolution of a solitary wave is provided by

$$\left.\begin{aligned} y &= H+\epsilon\tilde{\eta}, \\ \phi &= \Phi+\epsilon(\tilde{\phi}+\Phi_y\tilde{\eta}), \end{aligned}\right\} \tag{3.1}$$

where H and Φ are the surface displacement and velocity potential, respectively, of a steady solitary wave propagating in still water; $\tilde{\eta}$ and $\tilde{\phi}$ are the normal-mode perturbations to these quantities obtained by a linear stability calculation (Tanaka 1986). The small parameter ϵ is used to select the size of the initial perturbation. No generality is lost if we also normalize space and time so that the undisturbed fluid depth h and the acceleration due to gravity g are set equal to 1. With this normalization the basic solitary wave that was chosen for this study has an amplitude $a = 0.80374$. The corresponding phase speed c of this wave is 1.29400.

In order to study the growth of perturbations, we evaluated a perturbation integral or 'energy of perturbation' defined by

$$P(t) = \frac{1}{2}\int_{-\infty}^{\infty} \{y(x,t)-H(x-ct)\}^2\,\mathrm{d}x. \tag{3.2}$$

Tested on the undisturbed wave up to time $t = 10$, when the wave has propagated about thirteen times the undisturbed depth, $P(t)$ remains less than 10^{-10} in value. (Note, for comparison, that for the wave under consideration $\frac{1}{2}\int_{-\infty}^{\infty} H^2\,\mathrm{d}x = 0.44900$.) This extremely low value reflects the high accuracy with which the evolution of both disturbed and undisturbed waves can be calculated.

According to the linear stability calculation, there are two normal-mode perturbations for the steady solitary wave under consideration besides the trivial mode corresponding to a phase shift. One mode grows like $\mathrm{e}^{\lambda t}$ while the other decays like $\mathrm{e}^{-\lambda t}$ with $\lambda = 9.83\times10^{-2}$.

It is worth mentioning here the significance of the sign of the parameter ϵ. As shown in figure 1 the perturbation is not symmetric about $x = 0$, the initial position of the crest of the solitary wave. This implies that the perturbed wave has unequal slope on each side of the crest. Throughout this work we employ the convention that positive values of ϵ always perturb the steady wave such that the rear face of the wave is steeper than the front face, while negative values have the opposite effect. Although the sign of ϵ does not have any relevance to the linear theory, the long-time evolution of the perturbation is found to be completely different, as described in the next section.

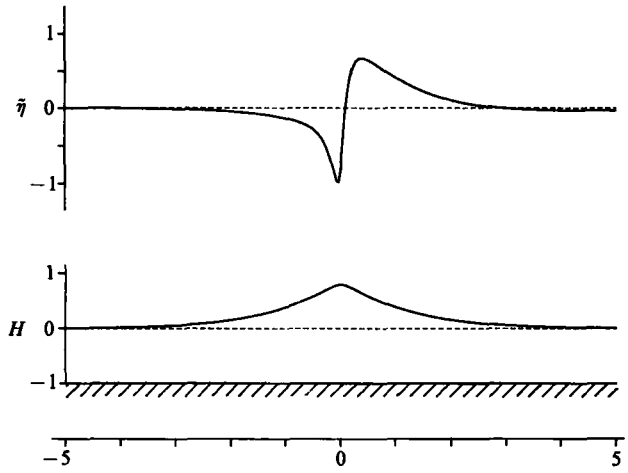

FIGURE 1. Growing normal-mode perturbation $\tilde{\eta}(x)$ for a solitary wave (shown beneath to natural scale) propagating from right to left. The decaying mode is given by $-\tilde{\eta}(-x)$.

Numerical calculations were performed for various values of $|\epsilon|$ ranging from 0.001 to 0.01. For these values of ϵ, the ratio r of the initial 'energy' of perturbation to that of the basic wave, defined as

$$r(\epsilon) = \frac{\int_{-\infty}^{\infty} \{\epsilon\tilde{\eta}(x)\}^2 \,\mathrm{d}x}{\int_{-\infty}^{\infty} H^2(x) \,\mathrm{d}x}, \tag{3.3}$$

varies from 6.75×10^{-7} to 6.75×10^{-5}.

With $\epsilon = \pm 0.001$, numerical results for the decaying mode are shown in figure 2(*a*), and for the growing mode in figure 2(*b*). The dashed lines show the linear stability predictions that the perturbation integral $P(t)$ should behave like

$$P(t) = \begin{cases} P(0)\exp(-2\lambda t) & \text{(decaying mode),} \\ P(0)\exp(+2\lambda t) & \text{(growing mode).} \end{cases} \tag{3.4}$$

The figures show good agreement between the results of the calculations and the predictions of the linear stability theory, providing an independent validation of the linear stability results.

We also calculated the initial growth rate λ_0, defined by

$$\lambda_0 = \frac{1}{2}\frac{\mathrm{d}}{\mathrm{d}t}\ln P(t)|_{t=0}, \tag{3.5}$$

for various values of ϵ. The result, shown in figure 3, clearly indicates a convergence to the value expected from the linear stability theory as $\epsilon \to 0$.

While the deviation from the basic wave remains sufficiently small, the two cases for the growing mode, corresponding to $\epsilon = +0.001$ and -0.001, both grow exponentially in time with almost the same growth rate, one slightly larger and one slightly smaller than predicted. However as time proceeds and the disturbances become larger, the growth rates diverge significantly. This more 'nonlinear' stage of the instability is discussed in the next section.

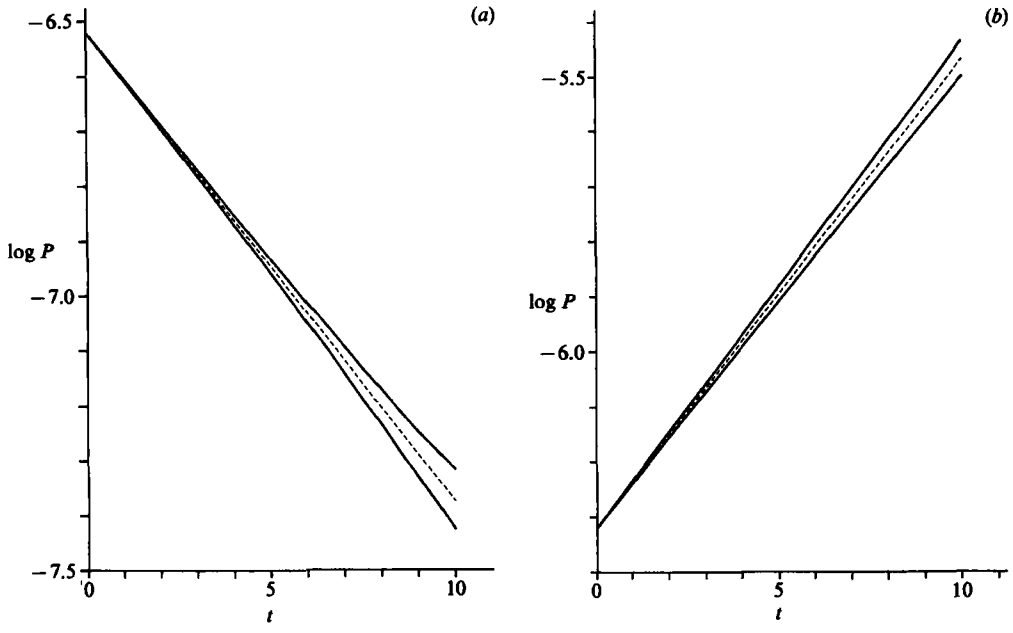

FIGURE 2. Development of the perturbation integral $P(t)$ for normal-mode perturbation with $\epsilon = 0.001$ (lower curve) and $\epsilon = -0.001$ (upper curve). The dashed line gives the exponential decay predicted by linear stability theory. (*a*) Decaying mode, (*b*) growing mode. Analysis for this decaying mode was suggested by Professor M. S. Longuet-Higgins.

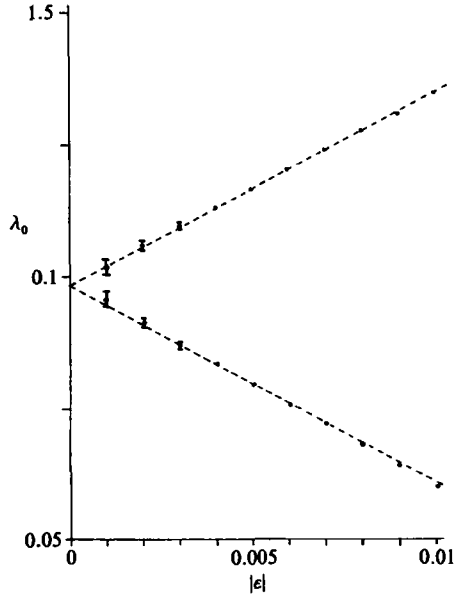

FIGURE 3. Initial growth rates λ_0 for the growing mode with $|\epsilon|$ between 0.001 and 0.01, showing the tendency towards the prediction of linear stability theory as $\epsilon \to 0$. The error bars are estimated from overall numerical errors. For small $|\epsilon|$, as in figure 2, the points lie close to the straight dashed lines.

4. Long-time evolution

In order to investigate the nonlinear stage of the instability, we calculated the evolution of the growing mode using the larger values for ϵ of 0.01 and -0.01. As shown in figure 4, the behaviour is quite different for the two cases: we shall discuss them separately.

4.1. *Breaking case* ($\epsilon = -0.01$)

The growth of the perturbation integral $P(t)$ is plotted only up to $t = 8.5$. Just after this time the wave showed signs of breaking (see figure 5) and the calculation could not be continued. The scale of the breaking region was found to be very small indeed and calculations failed when resolution of this region became inadequate. In figure 6 we have plotted the evolution of the maximum slopes on either side of the wave. This shows that the front face of the wave which was initially only slightly steeper than the rear face gradually steepens further until an almost singular growth in maximum slope occurs. It may be noted that the timescale of the breaking event seems much shorter than the characteristic timescale of the basic wave, which might be defined as $1/c = 0.7728$.

Longuet-Higgins & Cokelet (1978) investigated the nonlinear stage of the subharmonic instability for periodic waves on deep water and found in the same way that the instability eventually leads to breaking. Solitary waves and periodic waves on deep water lie at opposite extremes of the family of steady waves. The wavelength-to-depth ratio is ∞ for solitary waves and 0 for periodic waves on deep water. In spite of this great difference in the nature of the two cases, the local behaviour around the breaking crest shows some similarity. (Compare figure 5 of the present work and figures 15, 18 and 21 of Longuet-Higgins & Cokelet.) This fact supports their suggestion that the dynamics of the final stage of overturning are determined only by local conditions near the breaking crest.

Figure 7 shows the evolution of the shape of the perturbation $\tilde{y}(x,t)$ $(= y(x,t) - H(x-ct))$. It is evident that $\tilde{y}$ grows rapidly in a small region around the crest as the wave approaches overturning, and there are indications that this final stage of evolution occurs on a shorter timescale than the original growth of the perturbation.

4.2. *Non-breaking case* ($\epsilon = +0.01$)

Before we started this calculation, we naively believed that the growth of the unstable normal mode would always enhance the asymmetry of the perturbed wave and finally lead to breaking or some other drastic event. As discussed above this does happen for $\epsilon = -0.01$, but does not always happen.

In figure 8 we show the profile of the wave at $t = 100$ for the case $\epsilon = +0.01$. The normal mode that was superimposed on the steady solution is exactly the same as that used in the breaking case, the only difference being in the sign of ϵ. The evolution of the shape of the perturbation $\tilde{y}(x,t)$ and the maximum height $a(t)$ of the wave are shown in figures 9 and 10, respectively.

For this case the growth of the perturbation unexpectedly reduces the amplitude of the wave. The wave profile becomes more gentle as the perturbation grows. The asymmetry in the initial condition does not grow as it does for the breaking case and the wave remains almost symmetric throughout the evolution. The profile at $t = 100$ has been compared with that of the steady solitary wave of the same height; the two waves are graphically indistinguishable.

Bearing in mind that the initial perturbation integral $P(0)$ is less than 0.007% of

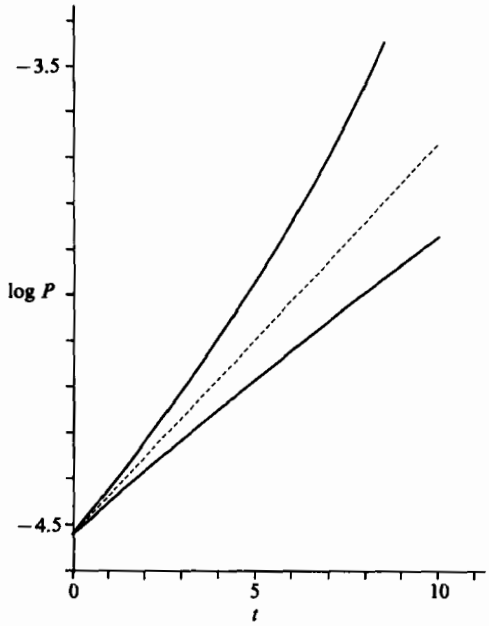

FIGURE 4. Curves as in figure 2 with $\epsilon = 0.01$ (lower curve) and $\epsilon = -0.01$ (upper curve). The upper branch leads to breaking at about $t = 8.9$.

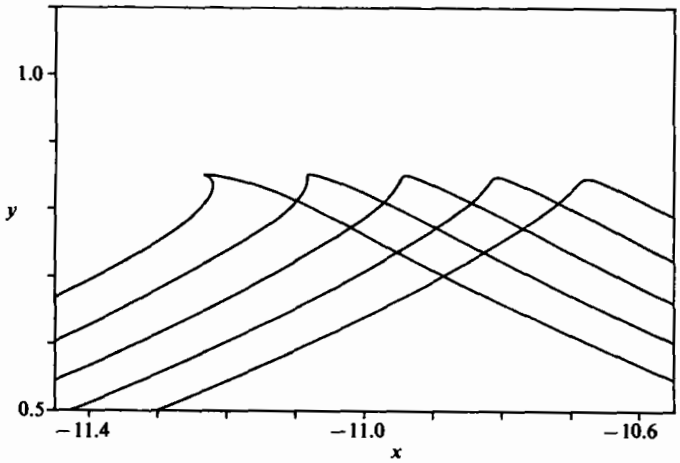

FIGURE 5. Overturning of the breaking wave crest ($\epsilon = -0.01$). Profiles are shown at times $t = 8.5$, 8.6, 8.7, 8.8 and 8.9.

the energy of the basic wave, it is surprising that the sign of the normal mode makes such a great difference to the long-time evolution of the instability.

The behaviour of the amplitude $a(t)$ shown in figure 10 suggests that the amplitude is exponentially approaching an asymptotic value. In order to estimate this value we applied one Shanks transformation to $a(t)$ defined by

$$S(a(t)) = \frac{a(t+\Delta t)a(t-\Delta t) - a^2(t)}{a(t+\Delta t) + a(t-\Delta t) - 2a(t)}. \tag{4.1}$$

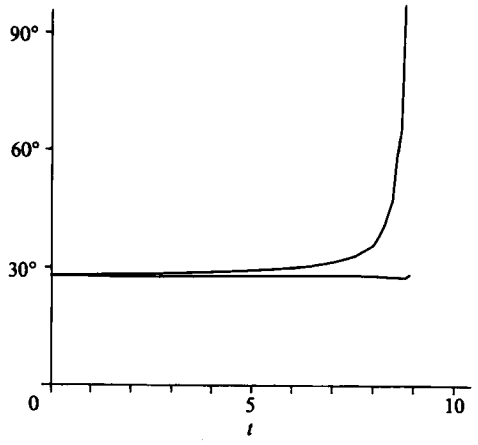

FIGURE 6. Maximum positive and negative slopes for the breaking case ($\epsilon = -0.01$), showing the rapid increase in slope of the front face through overturning.

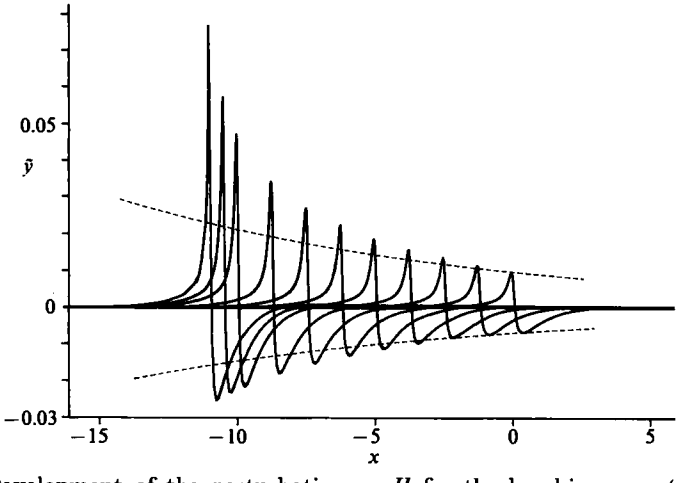

FIGURE 7. Development of the perturbation $y-H$ for the breaking case ($\epsilon = -0.01$) at times $t = 0$, 1, 2, 3, 4, 5, 6, 7, 8, 8.4 and 8.8. The dashed lines are the paths of maxima and minima as predicted by linear stability theory.

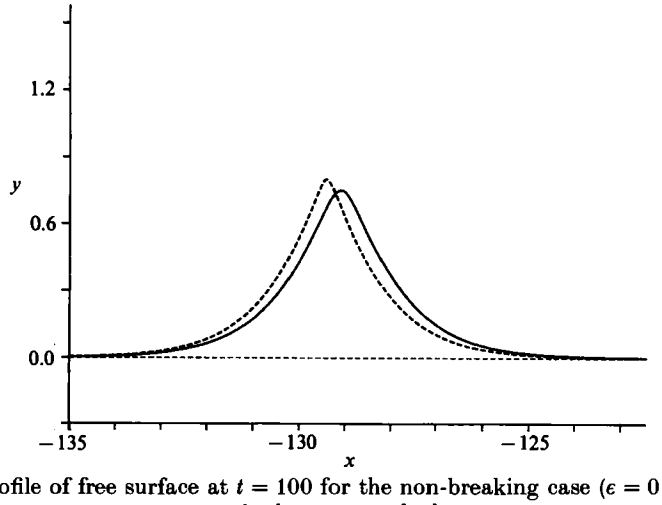

FIGURE 8. Profile of free surface at $t = 100$ for the non-breaking case ($\epsilon = 0.01$). The dashed line is the unperturbed case.

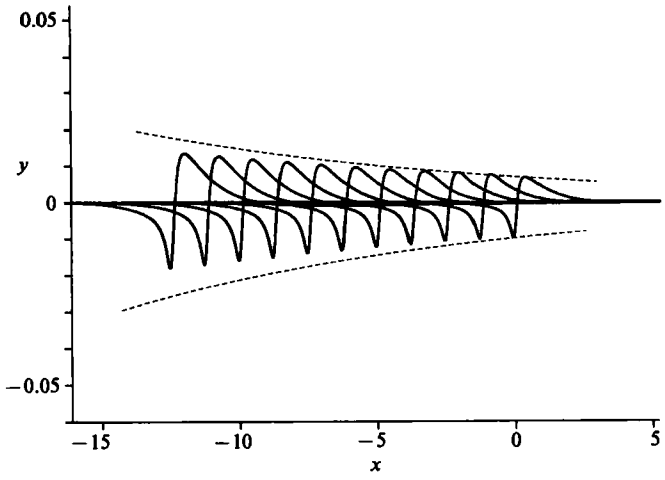

FIGURE 9. Curves as in figure 7 for the non-breaking case ($\epsilon = 0.01$) at times $t = 0$, 1, 2, 3, 4, 5, 6, 7, 8, 9 and 10.

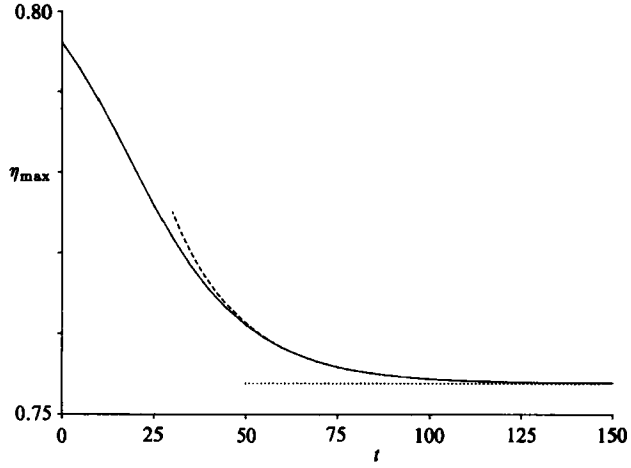

FIGURE 10. Evolution of the maximum height $a(t)$ of the wave for the non-breaking case ($\epsilon = 0.01$).

The result is shown in figure 11. Since the steady wave that we are employing as the basic wave is steeper than waves with the maximum of the total energy, total momentum (impulse) and excess mass, other steady solitary-wave solutions exist with exactly the same amounts of each of these quantities but with smaller amplitudes. We denote the amplitudes corresponding to the same amounts of energy, momentum and mass (as the initial perturbed solitary wave) by $\tilde{a}_e$, $\tilde{a}_i$ and $\tilde{a}_m$, respectively. (The values for the case studied are $\tilde{a}_e = 0.7539$, $\tilde{a}_i = 0.6938$ and $\tilde{a}_m = 0.6562$.) The result in figure 11 clearly shows that the wave evolution approaches the steady solitary wave with very nearly the same amount of total energy as the initial perturbed solitary wave.

There is an increase in magnitude of both the mass and momentum of the solitary wave. This is accounted for by the emission of two long waves. One is a radiated wave travelling in the opposite direction to the solitary wave. The other is a 'trailing' wave, following the solitary wave at nearly the linear wave speed. Despite the length

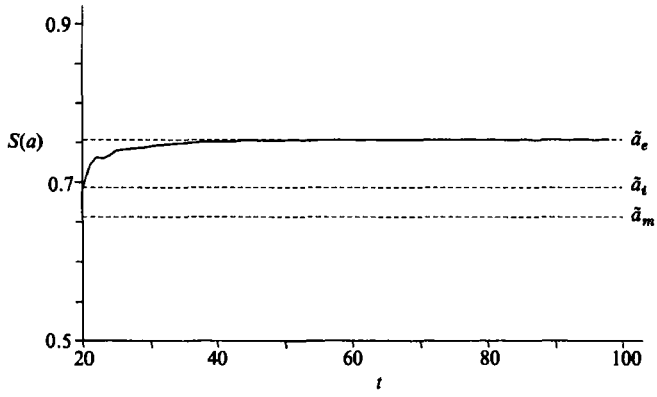

FIGURE 11. Estimated final height $S(a)$ of the emerging solitary wave (using Shanks transformation (4.1) with $\Delta t = 2$) compared with the wave heights for equivalent energy $\tilde{a}_e$, impulse $\tilde{a}_i$ and mass $\tilde{a}_m$.

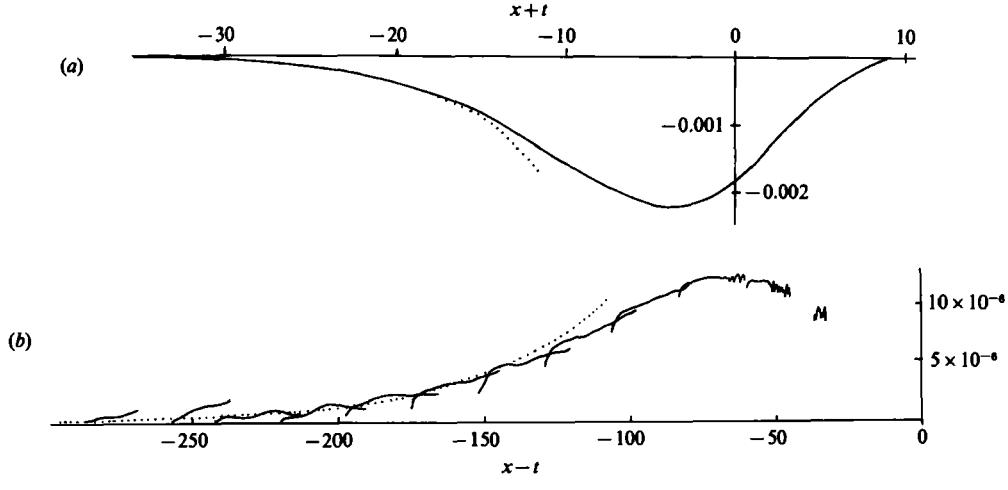

FIGURE 12. Elevation of (*a*) the trailing wave, (*b*) the radiated wave. For the radiated wave individual sections are shown to show those portions 'contaminated' by dispersive waves. Exponentials with exponents as in (4.6) are shown by dotted lines.

of the computational region having been limited to 53 times the depth these waves can be identified. Linear theory is used to build up sections of each wave from output at selected times. The surface elevation and horizontal velocity inserted into d'Alembert's solution for the linear long-wave equations give the trailing wave shown in figure 12(*a*). To define the radiated wave it is also necessary to subtract weak dispersive effects of the trailing wave. Note the very different vertical and horizontal lengthscales of the two waves.

The figure 12(*b*) for the radiated wave shows individual sections, since they give a clear idea of the accuracy of the results. For $(x-t) > -30$ the wave is masked by strong dispersive effects from short waves associated with the initial growth of the instability. The poor resolution of the radiated wave for $(x-t) < -240$ is due to the propagation of numerical errors caused when the peak of the trailing wave leaves the computational region. Only a simple truncation is used as the region is moved.

The wave profiles in figure 12 allow a check to be made on conservation of mass and momentum. The uncertainties in the radiated wave only allow measurement to the third decimal place. Mass and momentum are conserved to this accuracy, which corresponds to about 3% of the difference between the initial and final solitary waves.

Since the final solitary wave is stable, it might be thought that the observed exponential approach to the lower-amplitude solitary wave contradicts the findings of linear stability analysis. For t greater than about 60, we find that the wave profile evolves in the manner

$$y(x,t) \sim \tilde{H}(x+\tilde{c}t) + \mathrm{e}^{-\lambda t} G(x+\tilde{c}t) \tag{4.2}$$

as $t \to \infty$, where $\tilde{H}$ is the surface elevation of the final solitary wave, and G is a normal-mode perturbation. For 'stable' solitary waves, linear stability analyses have shown that no real growth/decay eigenvalue λ can exist for any disturbance function G which is finite in extent; that is $G(\theta)$ tends to zero as $\theta \to \pm\infty$.

However, it is clear that as $t \to \infty$ the disturbance function G that emerges from the numerical calculation we have performed does not necessarily tend to zero as $\theta \to +\infty$. If this condition for G is dropped, then for large values of $x+\tilde{c}t$ the profile in (4.2) must match with linear wave solutions of the form

$$y(x,t) \sim \eta_1(x+c_1 t) + \eta_2(x-c_2 t), \tag{4.3}$$

representing negatively and positively propagating disturbances with linear phase speeds c_1 and c_2. Matching of this with (4.2) for large values of $x+\tilde{c}t$ (where H can be neglected) is only possble if η_1 and η_2 are exponential functions, giving

$$\mathrm{e}^{-\lambda t} G(x+\tilde{c}t) \sim A\, \mathrm{e}^{\lambda(x+c_1 t)/(\tilde{c}-c_1)} + B\, \mathrm{e}^{\lambda(x-c_2 t)/(\tilde{c}+c_2)} \tag{4.4a}$$

or

$$G(x+\tilde{c}t) \sim A\, \mathrm{e}^{\lambda(x+\tilde{c}t)/(\tilde{c}-c_1)} + B\, \mathrm{e}^{\lambda(x+\tilde{c}t)/(\tilde{c}+c_2)} \tag{4.4b}$$

as $x+\tilde{c}t \to \infty$ with $x+c_1 t$ or $x-c_2 t$ fixed. Such unbounded behaviour for G (with A and B non-zero) is fully consistent with the evolution in (4.2), even for stable solitary waves. It may be noted that this argument would not be applicable to periodic waves.

Results for the time decay of amplitude, shown in figure 10, give the value $\lambda^{-1} = 19.2 \pm 0.5$ for the decay rate. The exponential corresponding to this decay rate is shown dashed in figure 10. The linear dispersion relation applied to η_1 and η_2, as given in (4.4a), requires that c_1 and c_2 satisfy

$$c_1^2 = \frac{\tilde{c}-c_1}{\lambda} \tan\frac{\lambda}{\tilde{c}-c_1}, \quad c_2^2 = \frac{\tilde{c}+c_2}{\lambda} \tan\frac{\lambda}{\tilde{c}+c_2}. \tag{4.5}$$

This leads to the values $c_1 = 1.0056 \pm 3$ and $c_2 = 1.000086 \pm 4$. The coefficients of the exponential growth rates with x of the trailing and radiated waves are therefore

$$\frac{\lambda}{\tilde{c}-c_1} = \frac{1}{5.47 \pm 0.15}, \quad \frac{\lambda}{\tilde{c}+c_2} = \frac{1}{44 \pm 1}. \tag{4.6}$$

Exponentials with these predicted coefficients are shown dotted in figure 12. The correspondence with the calculated trailing- and radiated-wave profiles is as good as can be expected from the accuracy of the calculations.

5. Conclusions

By applying the very efficient numerical method that has recently been developed by Dold & Peregrine, we have investigated the instability of a solitary wave on a fluid layer of constant depth.

The results of the linear stability calculation (Tanaka 1986) has been confirmed by evaluating the rate of growth of sufficiently small normal-mode perturbations.

In the nonlinear stage of the instability, two distinctive forms of evolution were found depending on the sign of the unstable normal-mode perturbation superimposed on the basic steady solution. In one case the instability leads directly to breaking as was expected. In the other case the growth of the perturbation leads to a monotonic decrease in the amplitude of the wave and the main part of the wave finally evolves into a new steady solitary wave which has almost the same amount of energy as the initial wave.

In the calculation shown above, the 'energy' of the initial perturbation relative to that of the steady wave was about 0.007%. As a result the difference between these two types of evolution becomes significant within a reasonable time. It is certain however that the two distinct forms of evolution would eventually be observed even for very small initial perturbations. Thus the nonlinear evolution of the system is *discontinuously* dependent on initial conditions. A very small change could completely alter the evolution of the system. Although sensitive dependence on initial conditions is not unusual in nonlinear systems, it may have important implications for our ability to predict whether or not a given unstable solitary wave will eventually break.

M. Tanaka thanks all the staff of School of Mathematics, University of Bristol for their hospitality. He also acknowledges the support from a UK Science and Engineering Research Council Visiting Fellowship which made his stay in Bristol possible. J. W. Dold also has SERC support and M. Lewy has NERC support.

REFERENCES

DOLD, J. W. & PEREGRINE D. H. 1986 An efficient boundary-integral method for steep unsteady water waves. In *Numerical Methods for Fluid Dynamics* II (ed. K. W. Morton & M. J. Baines), pp. 671–679. Clarendon.

LONGUET-HIGGINS, M. S. 1984 On the stability of steep gravity waves. *Proc. R. Soc. Lond.* A **396**, 269–280.

LONGUET-HIGGINS, M. S. & COKELET, E. D. 1978 The deformation of steep surface waves on water II. Growth of normal-mode instabilities. *Proc. R. Soc. Lond.* A **364**, 1–28.

NEW, A. L. 1983 On the breaking of water waves. Ph.D. dissertation, University of Bristol.

SAFFMAN, P. G. 1985 The superharmonic instability of finite-amplitude water waves. *J. Fluid Mech.* **159**, 169–174.

TANAKA, M. 1983 The stability of steep gravity waves. *J. Phys. Soc. Japan* **52**, 3047–3055.

TANAKA, M. 1985 The stability of sleep gravity waves. Part 2. *J. Fluid Mech.* **156**, 281–289.

TANAKA, M. 1986 The stability of solitary waves. *Phys. Fluids* **29**, 650–655.

ZUFIRIA, J. A. & SAFFMAN, P. G. 1986 The superharmonic instability of finite-amplitude surface waves on water of finite depth. *Stud. Appl. Maths* **74**, 259–266.